

---

# 浙江大学材料科学与工程学系本科生毕业论文编写规则

毕业论文(设计)是大学生从事科研工作成果的主要表现形式,是培养大学生的创新能力、实践能力和创业精神,实现人才培养目标的重要教学环节。同时毕业论文(设计)的质量也是衡量教学水平,审核学生毕业与学位资格的重要依据。

为了进一步加强毕业论文(设计)规范化及质量管理,不断提高本科生毕业论文(设计)质量,规范我系本科生毕业论文的撰写和编辑格式,根据《科学技术报告、学位论文和学术论文的编写格式》(GB/T 7713-1987)和《学位论文编写规则》(GB/T 1.1—2000---审批版),制定本本科生毕业论文编写规则。其中参考文献著录规则根据 GB/T 7714-2005 的标准撰写。

本科生毕业论文(设计)书面材料主要包括文献综述与开题报告、外文文献翻译、学位论文三部分,其中学位论文是最主体的部分。由于三者格式要求类似。故此本科生毕业论文编写规则首先将详细阐述学位论文的结构、规范与要求,再对文献综述与开题报告、外文文献翻译两部分进行补充说明。

## 一. 学位论文基本结构

学位论文基本结构包括前置部份、主体部份和结尾部份。总字数在 1 万字以上。

### 1.1 前置部份包括：

- (1) 封面
- (2) 英文题名页
- (3) 勘误页(可根据需要)
- (4) 序言或前言(可根据需要)
- (5) 摘要页
- (6) 英文摘要页(abstract)
- (7) 目次页

### 1.2 主体部份：

- (1) 引言(绪论)

- 
- (2) 正文
  - (3) 结论

### 1.3 结尾部分：

- (1) 参考文献
- (2) 致谢
- (3) 附录(可根据需要)
- (4) 索引(根据需要)
- (5) 攻读学位期间发表的学术论文与取得的其它研究成果（根据需要）
- (6) 封底

## 二. 学位论文编写规范与要求

### 2.1 前置部分

1. **封面**：封面包括校名、学校徽标、学位论文题目、作者姓名与学号、导师姓名、年级与专业、学科和专业名称、提交时间等内容。采用学院规定的统一格式模板。

其中论文题目应准确概括整个论文的核心内容，简明扼要，一般不能超过25个汉字，必要时可以加副标题。学科和专业名称必须按国家本科生培养的学科专业目录，规范填写。其他具体格式参照附件1：学位论文封面格式。

2. **英文题名页**：英文题名页包括学位论文英文题目、作者姓名、导师职称及姓名、毕业设计所在单位名称、提交日期等。采用学院规定的统一格式模板。

其中英文题目翻译应简短准确，一般不应超过150个字母。姓名为中文全拼，按姓后名前的书写格式。其他具体格式参照附件2：英文提名页样式。

3. **序言或前言**：学位论文的序言或前言，一般是作者对本篇论文基本特征的简介，如说明研究工作缘起、背景、主旨、目的、意义、编写体例，以及资助、支持、协作经过等。这些内容也可以在正文引言（绪论）中说明。

4. **中文摘要**：摘要是论文内容的总结概括，应简要说明论文的研究目的、基本研究内容、研究方法、创新性成果及其理论与实际意义，突出论文的创新之处，语言力求精练。不宜使用公式、图表，不标注引用文献。本科生毕业论文(设计)摘要的字数在300以内。摘要最后另起一行，列出4—8个关键词。关键词应体现论文特色，具有语义性，在论文中有明确的出处。并应尽量采用《汉语主题词表》或各专业主题词表提供的规范词。

---

5. **英文摘要(abstract)**：英文摘要应与中文摘要内容相对应。

6. **目次页**：论文中内容标题的集合。包括目录之后所有的大标题，如：插图与附表清单、参考文献、注释、索引、致谢等，以及章节序号和名称，等等。排在英文摘要之后另起页。无页眉页码。其他具体格式参照附件3：目次页样式。

英文题名页之后与目次页之前中间部分(序言或前言、中文摘要、英文摘要)用罗马数字单独编连续码，单面复印时页码排在页脚居中位置，双面复印时页码分别按左右侧排列。

每一项内容均须另起页(置于单页码页上，下同)。

## 2.2 主体部份

包括引言(绪论)、正文和结论。主体部分应从另页右页开始，论文正文部分字数在8000字以上。

### 2.2.1 一般要求

#### 1. 引言(绪论)

引言独立成章。应包括论文的研究目的，流程和方法等。论文研究领域的历史回顾，文献回溯，理论分析等内容，用足够的文字叙述。

#### 2. 正文

论文正文是主体，研究课题的性质不同，在选题、研究方法、结果表达方式等方面有很大的差异，不能作统一的规定。一般论文正文可包括综述、理论分析、计算方法、实验装置和制备测试方法、实验结果、数据分析和讨论、个人的论点和研究成果、结论及意义等。论文应层次分明、数据可靠、图表规范、文字简炼、说明透彻、推理严谨、立论正确，避免使用文学性质的带感情色彩的非学术性词语。论文中如出现非通用性的新名词、新术语、新概念，应作相应解释。文中若有与导师或他人共同研究的成果，必须明确指出；如果引用他人的结论，必须明确注明出处，并与参考文献一致。

**图**：图应具有“自明性”。图题应简单明了。图包括曲线图、构造图、示意图、框图、流程图、记录图、地图、照片等，应鲜明清晰。照片上应有表示目的物尺寸的标度。如果图中含有几个不同部分，应将分图号标注在分图的左上角，并在图题中列出各部分内容，

**表**：表应具有“自明性”。表题应简单明了，表中参数应标明量和单位的符号；表的编排，一般是内容和测试项目由左至右横读，数据依序竖读。如某个表需要转页接排，在随后的各页上应重复表的编号。编号后跟上表题(可省略)和“(续)”，置于表上方。续表均应重复表头。

---

图、表中的术语、符号、单位等应与正文表述所用一致。图、图题，表、表题位于同一页中，不可分开。

**公式：**公式中用到的量必需在正文中说明其物理意义。

**引文标** 悼砥 \ 泊罨5 筵表般社豁 l m x 公溝多 E 祉 葦 f P < 题梳 晦+

---

下方。序号均加粗，与题间空一个汉字符位。中文采用五号仿宋体字，英文用Times New Roman体10.5磅，居中书写，单倍行距，段前6磅，段后12磅。论文中的公式应另行起，并缩格书写。公式编号置于括号内，右端对齐，公式与编号之间可用“...”连接。较长的公式需要转行时，应尽可能在“=”处回行，或者在“+”、“-”、“×”、“/”等记号处回行。图、表、公式等与正文之间要有一定的行间距。

#### 4. 数字、标点符号

文中阿拉伯数字均用 Times New Roman 体，文中的标点符号则依其所在位置来确定字体，英文段落中使用 Times New Roman 体，中文段落中使用仿宋体。

#### 2.2.3 页码、页眉、脚注编写规则

学位论文的页码，正文和后置部分用阿拉伯数字编连续码。单面复印时页码排在页脚居中位置，双面复印时页码分别按左右侧排列。

页眉、页脚文字中文采用小五号宋体，英文采用10.5磅Times New Roman体，单倍行距。页眉文字居中，论文正文左侧页眉为“浙江大学学士学位论文”，右侧为章标题；论文后置部分页眉内容与该部分的大标题一致（具体请参考相关附件）；页眉下横线可为单横线也可用上粗下细文武线。脚注文字单倍行距，顶左，首行缩进两个字符。

#### 2.2.4 引文标注格式

论文中引用的文献的标注方法遵照 GB/T 7714 - 2005，可采用顺序编码制，也可采用著者 - 出版年制。

##### 顺序编码制：

1. 按正文中引用的文献出现的先后顺序用阿拉伯数字连续编码，并将序号置于方括号中，以上标形式放在文献作者或句子的末尾。

2. 同一处引用多篇文献时，将各篇文献的序号在方括号中全部列出，各序号间用逗号，如遇连续序号，可标注起讫号“-”，例如：

王材料<sup>[1]</sup>指出.....，李材料<sup>[2-4]</sup>认为.....，提出了多种理论模型<sup>[2, 5, 10-12]</sup>。

3. 同一文献在论著中被引用多次，只编1个序号，文献表中不再重复著录。例如：

张材料等<sup>[5]</sup>.....。

.....

张材料等<sup>[5]</sup>指出.....。

##### 著者-出版年制：

1. 正文引用的文献采用著者-出版年制时，各篇文献的标注内容由著者姓氏与出版年构成，并置于“( )”内，放在正文中引用了该文献的句子末尾。倘若

---

只标注著者姓氏无法识别该人名时，可标注著者姓名。集体著者著述的文献可标注机关团体名称。倘若正文语句中已提及著者姓名，则在其后的“（ ）”内只须著录出版年。例如：……（张材料, 2006），……张材料（2006）认为……。

2. 引用多著者文献时，对欧美著者只需标注第一个著者的姓，其后附“et al”；对中国著者应标注第一著者的姓名，其后附“等”字，姓名与“等”字之间留1个空格。例如：……（张材料 等, 2005）……。

在参考文献表中著录同一著者在同一年出版的多篇文献时，出版年后应用小写字母a, b, c...区别。例如：

Kennedy W J, Garrison R E. 1975a. Morphology and genesis of nodular chalks and hardgrounds in the Upper Cretaceous of southern England. *Sedimentology*, 22:311-386.

Kennedy W J, Garrison R E. 1975b. Morphology and genesis of nodular phosphates in the Cenomaman of South-east England. *Lathiaia*, 8:339-360.

3. 正文中多次引用同一著者的同一文献时，在正文中标注著者与出版年，并在“（ ）”外以上标形式标注引文页码。例如：

……（张材料等, 2005）。

……

……张材料等（2005）认为……。

## 2.3 结尾部分

结尾包括包括参考文献、附录、索引、致谢和攻读学位期间发表的学术论文与取得的其它研究成果等。每一项内容均须另起页。

### 2.3.1 参考文献

#### 1. 基本要求

参考文献表是文中引用的有具体文字来源的文献集合，其著录项目和著录格式遵照GB/T 7714 - 2005的规定执行。要求查阅与毕业论文（设计）相关的文献8-10篇以上，其中外文文献不少于3-5篇。

参考文献表应置于正文后，并另起页。所有被引用文献均要列入参考文献表中，严禁论文抄袭现象的发生。引文采用顺序编码标注时，参考文献表按编码顺序排列，引文采用著作 - 出版年制标注时，参考文献表应按著者字顺和出版年排序。建议根据《中国高校自然科学学报编排规范》的要求书写参考文献，并按顺序编码制，即按中文引用的顺序将参考文献附于文末。

#### 2. 文献类型、电子文献载体类型及其标志代码说明

电子文献类型和载体类型标志是必备的著录项目。非电子文献类型可以省略。

学位论文类型的文献必须明确标注。中文硕士学位论文标注[硕士学位论文]，中文博士学位论文标注[博士学位论文]，外文学位论文标注[D]。

国标GB/T 7714—2005列出的文献类型标志如下：普通图书M，会议录C，汇编G，报纸N，期刊J，学位论文D，报告R，标准S，专利P，数据库DB，计算机程序CP，电子公告EB。

会议录C指座谈会、研讨会、学术年会等会议的文集；汇编G指多著者或个人著者的论文集；S标志的文献还包括政策、法律、法规等文件。

电子文献载体类型标志如下：磁带MT，磁盘DK，光盘CD，联机网络OL。

### 3. 参考文献格式

几种主要参考文献（学术期刊、专（译）著、学位论文、专利、技术标准、电子文献等）的著录项目与格式要求如下。所有作者姓名均须列出，不可用“et al”或者“等”代替。中文姓名姓前名后，英文名字一律采用姓后名前的著录形式。

**学术期刊：**（其标志代码可以省略）[序号] 作者 文题 刊名 年 卷号（期号） 起止页码

示例如下：

[1] T. Kimura, T. Goto, H. Shintani, K. Ishizaka, T. Arima, and Y. Tokura. Magnetic Control of Ferroelectric Polarization. *Nature*, 2003, 426(6962): 55-58.

[2] 陈浩元. 著录文后参考文献的规则及注意事项. *编辑学报*. 2005, 12(6):413-415.

**专（译）著：**[序号] 作者（译者） 书名. 出版地：出版者，出版年，起止页码

示例如下：

[3] 钟维烈. 铁电体物理学. 北京：科学出版社，1996:37-39.

[4] C. 基泰尔. 固体物理导论. 项金钟，吴兴惠，译. 8版. 北京：化学工业出版社，2005: 22-24.

**学位论文：**（其标志代码必须标注）[序号] 作者 文题 [XX学位论文] 授予单位所在地：授予单位 授予年份 起止页码

示例如下：

[5] 张材撝 軒 | P 览 P \*滴学位论文].

---

[6] 张材料. 一种XXXX多功能材料: 中国, xxxxxxxx.x. 2009-04-18.

**技术标准:** (其标志代码可以省略) [序号] 发布单位技术标准代号 技术标准名称 出版地: 出版者, 出版日期

示例如下:

[7] 全国信息与文献工作标准化技术委员会出版物格式分委员会. GB/T 12450-2001 图书书名页. 北京:中国标准出版社, 2002.

**电子文献:** (其标志代码必须标注) [序号] 主要责任者. 题名: 其他题名信息[文献类型标志/文献载体标志]. 出版地: 出版者, 出版年(更新或修改日期) [引用日期]. 获取和访问路径(联机文献必备).

示例如下:

[8] 萧钰. 出版业信息化迈入快车道[EB/OL]. (2001-12-19) [2002-04-15]. <http://www.creader.com/news/200112190019.htm>.

[9] Online Computer Library Center, Inc. History of OCLC[EB/OL]. [2000-01-08]. <http://www.oclc.org/about/history/default.htm>.

[10] Scitor Corporation. Project scheduler[CP/DK]. Sunnyvale, Calif.: Scitor Corporation, c1983.

### 2.3.2 附录

附录作为主体部分的补充,并不是必须的。附录依次为附录1,附录2等。附录中的图表公式另编排序号,与正文分开。

下列内容可以作为附录编于论文后:

为了整篇论文材料的完整,但编入正文又有损于编排的条理性和逻辑性,这一材料包括比正文更为详尽的信息、研究方法和技术更深入的叙述,对了解正文内容有用的补充信息等;

由于篇幅过大或取材于复制品而不便于编入正文的材料;

不便于编入正文的罕见珍贵资料;

对一般读者并非必要阅读,但对本专业同行有参考价值的资料。

**2.3.3 索引:** 根据需要可以编排分类索引,关键词索引等。

**2.3.4 致谢:** 致谢对象限于对课题研究、学位论文完成等方面有较重要帮助的单位和个人。

**2.3.5 攻读学位期间发表的学术论文与取得的其他研究成果:** 按学术论文发表的时间顺序,列齐本人在攻读学位期间发表或已录用的学术论文清单。其他研究成果可以是申请的专利、获得的奖项及完成的项目等。如果没有,则省略此内容。



## 三. 学位论文排版和印刷要求

### 3.1 纸张要求和页面设置

	要求
纸张	A4 (210×297), 幅面白色
页面设置	上、下2.54cm, 左、右3.17cm, 页眉1.5cm、页脚1.75cm, 装订线0cm, 封面上、下3.8cm, 左、右3.2cm, 页眉页脚3.0cm
页眉	宋体, 小五号字, 居中, Abstract部分用Times New Roman体10.5磅
页码	仿宋体, 五号, 单面复印居中, 双面复印则按左右排列。

### 3.2 封面

	中文要求
论文题目	仿宋体, 小二号字, 加粗(可分两行), 单倍行距
申请人姓名与学号	仿宋体, 四号字, 单倍行距
指导教师	同上
专业名称	同上
所在院系	同上
论文提交日期	用简体汉字, 不用阿拉伯数字, 仿宋体, 小三号字

### 3.3 英文题名页

	要求
论文题目	New Times Roman体, 16磅, 加黑, 居中, 行距30磅
申请人姓名	同上
指导教师	同上
毕设所属单位	Time New Roman, 14磅, 居中, Bold
论文提交时间	Time New Roman, 14磅, 居中

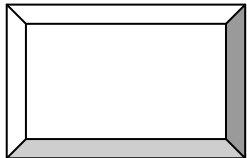
### 3.4 摘要和关键词

	中文摘要	英文摘要
标题	摘要：二字间空一个汉字字符位，仿宋体，三号字，加粗，居中，单倍行距，段前24磅，段后18磅	Abstract：New Times Roman, 16磅，加粗，居中，单倍行距，段前24磅，段后18磅
段落文字	仿宋体，小四号，两端对齐书写，段落首行左缩进2个汉字。行距20磅，段前段后0磅	Times New Roman 12磅，两端对齐书写，段落首行左缩进2个英文字符。行距20磅，段前段后0磅
关键词	同上，“关键词”三字加粗	同上，“Keywords”加粗

### 3.5 目录

	示例	要求
标题	目 录	二字间空一个汉字字符位，仿宋体，三号字，加粗，居中，单倍行距，段前24磅，段后18磅
各章目录	第一章 绪论.....1	仿宋体，小四号字，单倍行距，段前6磅，段后0磅，两端对齐，页码右对齐
一级节标题目录	1.2 文献概述.....10	仿宋体，小四号字，单倍行距，左缩进1个汉字，段前6磅，段后0磅，两端对齐，页码右对齐
二级节标题目录	1.2.3 尚待解决的问题...10	仿宋体，五号字，单倍行距，左缩进2个汉字，段前6磅，段后0磅，两端对齐，页码右对齐

### 3.6 正文

	示 例	要 求									
各章标题	<b>第一章</b> ×××	仿宋体，三号字，加粗，居中，单倍行距，段前24磅，段后18磅，章序号与章名间空一个汉字符									
一级节标题	<b>1.2</b> ××××	仿宋体，四号字，加粗，顶左，单倍行距，段前24磅，段后6磅，节序号与题名间空一个汉字符									
二级及以下节标题	<b>1.2.1</b> ×××	仿宋体，小四号字，顶左，单倍行距，段前12磅，段后6磅，节序号与题名间空一个汉字符									
段落文字	<p>××××××××××××</p> <p>××</p> <p>××××××××××××</p> <p>××</p>	仿宋体，小四号字（英文用Times New Roman体12磅），两端对齐书写，段落首行左缩进2个汉字符。段前段后0磅，行距20磅（段落中有数学表达式时，可根据表达需要设置该段的行距）									
图序、图名、图注	 <p><b>图2.1</b> ×××</p>	置于图的下方，仿宋体，五号字，居中，单倍行距，段前6磅，段后12磅，图序与图名文字之间空一个汉字符位，图序加粗。图注位于图名下方，标题加粗，左缩进两个汉字符，续行悬挂缩进左对齐，两端对齐，英文图题用Times New Roman体，10.5磅									
表序、表名、表注	<p><b>表2.1</b> ×××</p> <table border="1" data-bbox="427 1563 699 1729"> <tr> <td></td> <td></td> <td></td> </tr> <tr> <td></td> <td></td> <td></td> </tr> <tr> <td></td> <td></td> <td></td> </tr> </table>										置于表的上方，仿宋体，五号字，居中，单倍行距，段前6磅，段后6磅，表序与表名文字之间空一个汉字符位，表序和表注标题加粗，表注左缩进两个汉字符，续行悬挂缩进左对齐，两端对齐，英文表题用Times New Roman体，10.5磅
表达式	<b>**/*=**..... (3.2)</b>	表达式居中排，序号加圆括号，仿宋体，五号字，右顶格排									

### 3.7 其他

	要求
符号说明	标题字体字号等同论文正文，说明部分：仿宋体，五号字（英文用Times New Roman体10.5磅），行距16磅，段前段后0磅
参考文献	“参考文献”仿宋体，三号字，加粗，居中，单倍行距，段前24磅，段后18磅。注录部分：仿宋体，五号字（英文用Times New Roman体10.5磅），行距20磅，段前段后0磅；中英文一率用正体；续行缩进两个字符两端对齐
附录	标题同参考文献，内容部分：仿宋体，小四号字（英文用Times New Roman体12磅），两端对齐书写，段落首行左缩进2个汉字符。段前段后0磅，行距20磅（段落中有数学表达式时，可根据表达需要设置该段的行距）
致谢	标题：二字间空一个汉字字符位，其它同参考文献。内容部分等同论文正文
个人简历	标题同参考文献。正文部分等同论文正文
攻读学位期间学术成果	标题要求同各章标题，正文部分：仿宋体，小四号字（英文用Times New Roman体12磅），行距20磅，段前段后0磅，学术论文书写格式同参考文献

### 3.8 印刷及装订要求

论文封面使用浙江大学材料科学与工程学系统一印刷封面。自中文摘要起双面印刷，之前部分单面印刷。论文必须用线装或热胶装订，不使用钉子装订。

## 四. 文献综述与开题报告的结构、规范与要求

文献综述与开题报告主要包括封面、目录、正文、参考文献四部分。正文部分包括课题研究背景与意义、研究现状、存在问题与本课题的提出、课题研究方案与实施计划、课题研究预期结果五项内容。下面将分别进行说明。

### 4.1 封面

封面由学校统一设计，内容与要求和学位论文基本相同。具体格式参照附件12：文献综述与开题报告封面格式。

---

## 4.2 目录

格式排版要求与学位论文目录相同，具体格式参照附件 13。

## 4.3 正文

正文首先写上文献综述和开题报告的标题，字体为黑体、小二、加粗，居中、单倍行距、段前 24 磅段后 18 磅。正文中文献综述（包括课题研究的背景与意义、研究现状等）内容要切题，要求字数各 3000 字以上。开题报告（包括存在的问题与本课题的提出、课题研究方案与实施计划、课题研究预期结果等）字数要求 3500 字以上。

正文另起一页。不分章，新的第一层次不需要另起一页。第一层次标题用汉字标号，如“一”，格式与学位论文正文标题相同。其他层次的标号规则、格式要求，以及正文中段落、图、表、公式、引文标号、注释等与学位论文正文相同。

正文文献综述部分奇数页页眉为书写“浙江大学学士学位论文文献综述与开题报告”。页眉的偶数页书写文献综述与开题报告的题目。页码编排方式与学位论文相同。具体格式参照附件 14。

### 4.3.1 课题研究背景与意义

这部分需要阐述与所选课题的历史背景，其引起人们关注的应用前景和或者基础物理意义。

### 4.3.2 研究现状

这部分需要阐述所选课题在相应学科领域中的发展进程和研究方向，特别是近年来的发展趋势和最新成果（观点、理论、实践成就等）。通过与中外研究成果的比较和评论，说明自己的选题是符合当前的研究方向并有所进展，或采用了当前的最新技术并有所改进，目的是使读者进一步了解本课题的意义。

### 4.3.3 存在的问题与本课题的提出

此部分阐述相应学科领域中不清楚或者未解决的问题，指出不足之处和有待于进一步探索的方面，说明人们是从哪几个方面去研究和论述这些问题的。进而列出本课题研究要解决的核心问题，在研究中采取的新思路，尝试的新方法所具有的实践和理论意义（即创新点）。

### 4.3.4 课题研究方案与实施计划

此部分首先阐明研究的基本内容（论文框架）、理论思考过程、制备与性能

---

测试方案、工作计划与时间安排等。然后列出本研究已经具备的条件，如硬件和软件、主观和客观等等，列出本研究需要提供的支持和可能遇到的困难，综合各因素做一个的可行性分析，确保毕业设计能够按期完成。

#### 4.3.5 课题研究预期结果

阐述课题研究预期结果，即研究有可能在某一或者某些方面取得怎样的创新性成果。

#### 4.4 参考文献

文献综述和开题报告中所引用的所有文献集合。格式和学位论文中参考文献格式相同。

### 五. 外文文献翻译的规范与要求

所选文献必须是参考文献当中的 1 篇，且文献内容与论文内容相关性最大，译后汉字不少于 3000 字。译文的层次标号按原文照抄，但格式与学位论文正文要求相同。译文中图、表、引文标注、对正文补充说明的注释标注等按原文照抄。段落、图、表、公式、引文标号、对正文补充说明的注释等格式要求与学位论文正文要求相同。文章作者、参考文献、非对正文补充说明类注释、致谢等内容不用翻译。外文文献原文以 PDF 的格式置于译文后面。

具体格式参照附件 15：外文文献翻译格式。

**附录：浙江大学材料科学与工程学系学位论文撰写格式范例**

---

( )

---

**A Dissertation Submitted to Zhejiang University for  
Bachelor Degree of Engineering**

统一印刷



统一印刷,Time New Roman, 16 磅

Title, Time New Roman,16  
磅,Bold , 居中

---

Submitted by

统一印刷,Time New  
Roman, 16 磅 , 居中

Time New Roman

**San Zhang**

Supervised by

**Prof. Si Li**

**Department of material Science and Engineering  
Laboratory of Dielectric Materials, Zhejiang University, Hangzhou  
People's Republic of China**

June, 2th, 2010





---

页眉：偶数页内容为“浙江大学学士学位论文”，宋体，小五号字，居中





附件 5：目次页示例

另起一页（为简略，此节及之后节示例中空白偶数页均省略，毕业论文中不可省。）

目 录

标题：二字间空一个汉字字符，仿宋体，三号字，加粗，居中，单倍行距段前 24 磅，段后 18 磅

勘误表.....	章标题：仿宋，小四号字，单倍行距，段前 6 磅，段后 0 磅，两端对齐，页码右对齐	.....I
序言（前言）.....		.....
插图和附表单.....		.....
缩写、符号清单、术语表.....		.....
第一章 引言（绪论）.....	一级节标题：仿宋体，小四号字，左缩进一个汉字字符，单倍行距，段前 6 磅，段后 0 磅，页码右对齐	.....1
1.1（第1章第1节）题名.....		.....3
第二章 题名.....		.....5
2.1（第2章第1节）题名.....		.....7
2.1.1（二级节标题）题名.....	二级节标题：仿宋体，五号字，左缩进两个汉字字符，单倍行距，段前 6 磅，段后 0 磅，页码右对齐	.....8
2.2（第2章第2节）题名.....		.....10
.....		
结论.....		.....41
参考文献.....		.....60
致谢.....		.....67
附录A.....		.....68
附录B.....		.....69
索引.....		.....70
攻读学位期间发表的学术论文与取得的其他研究成果.....		.....72















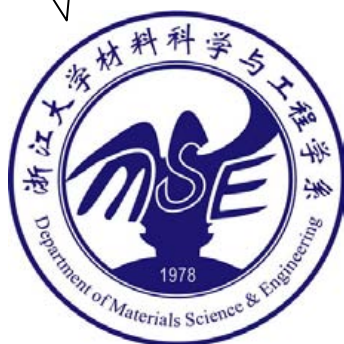






附件 11: 学位论文封底格式

统一印刷



黑体，四号字，居中，  
段前 24 磅段后 18 磅，  
单倍行距。

附件 12:文献综述和开题报告封面

统一格式，单面印刷

浙江大學

统一印刷

统一印刷，黑体，  
一号字，加粗



统一印刷

此列统一印刷，华文仿宋，  
三号字，加粗

仿宋，三号字，加粗

---

---

---

---



# 目 录

开始双面印刷，格式与学位论文目次页相同	1
1.1 题名	3
二 研究现状	5
2.1 (二级节标题) 题名	7
2.1.1 (三级节标题) 题名	8
2.2 (二级节标题) 题名	10
三 存在的问题与本课题的提出	18
四 课题研究方案与实施计划	24
4.1 样品制备	24
4.2 性能测试	26
4.2.1 ××测试	26
4.2.2 ××测试	27
4.3 进度安排	26
五 研究预期结果	28
参考文献	29











# Direct imaging of hydrogen-atom columns in a crystal by annular bright-field electron microscopy

Ryo Ishikawa<sup>1</sup>, Eiji Okunishi<sup>2</sup>, Hidetaka Sawada<sup>2</sup>, Yukihiro Kondo<sup>2</sup>, Fumio Hosokawa<sup>2</sup> and Eiji Abe<sup>1\*</sup>

Enhancing the imaging power of microscopy to identify all chemical types of atom, from low- to high-atomic-number elements, would significantly contribute for a direct determination of material structures. Electron microscopes have successfully provided images of heavy-atom positions, particularly by the annular dark-field method<sup>1,2</sup>, but detection of light atoms was difficult owing to their weak scattering power. Recent developments of aberration-correction electron optics<sup>3-5</sup> have significantly advanced the microscope performance, enabling identification of individual light atoms such as oxygen<sup>6-9</sup>, nitrogen<sup>7,9</sup>, carbon<sup>9-11</sup>, boron<sup>9</sup> and lithium<sup>12,13</sup>. However, the lightest hydrogen atom has not yet been observed directly, except in the specific condition of hydrogen adatoms on a graphene membrane<sup>14</sup>. Here we show the direct imaging of the hydrogen atom in a crystalline solid  $\text{YH}_2$ , based on a classic 'hollow-cone' illumination theory<sup>15-18</sup> combined with state-of-the-art scanning transmission electron microscopy. The optimized hollow-cone condition derived from the aberration-corrected microscope parameters confirms that the information transfer can be extended to  $22.5 \text{ nm}^{-1}$ , which corresponds to a spatial resolution of about  $44.4 \text{ pm}$ . These experimental conditions can be readily realized with the annular bright-field imaging in scanning transmission electron microscopy<sup>19,20</sup> according to reciprocity<sup>21</sup>, revealing successfully the hydrogen-atom columns as dark dots, as anticipated from phase contrast of a weak-phase object<sup>22</sup>.

Instead of a conventional axial illumination, a hollow-cone illumination (HCI) employs a series of off-axial illuminations over certain angle ranges of incident beams (Fig. 1a). In the early studies of optics, it was already shown that HCI is able to improve significantly the resolution as well as signal-to-noise ratio of a phase contrast<sup>15-17</sup> (intensity due to wave interferences) by eliminating the effect of wavelength fluctuations of the incident beam<sup>23</sup>, that is, a chromatic aberration ( $C_c$ ) that causes the focus instability. As  $C_c$  is a primary factor that limits the resolution of the phase-contrast imaging in transmission electron microscopy (TEM), the use of HCI for TEM has been attempted by several researchers<sup>16-18,24</sup>. It was demonstrated that, compared with axial illumination, the achievable resolution of HCI can be almost doubled with the optimized conditions, which are derived on the basis of the phase-contrast transfer function (PCTF) of HCI TEM (ref. 18). It was in turn shown that, according to reciprocity<sup>21</sup>, HCI TEM can be equivalently realized by locating an annular detector within the bright-field region (namely, the direct-beam disc) in scanning transmission electron microscopy (STEM) (ref. 20); see the ray paths in Fig. 1a. This is termed annular-bright-field (ABF) imaging<sup>7,15</sup>, which is well in accordance with the well-known annular-dark-field (ADF) imaging<sup>1,2</sup> in STEM. The fundamentals of HCI-related TEM/STEM imaging were established

as the Rose Cowley method by their pioneering works; though, their experimental demonstrations were strongly restricted by insufficient microscope performance at that time. It is noteworthy that, to realize stable instrumentations, ABF STEM may be advantageous rather than dynamic HCI TEM (ref. 24), which requires continuous and precise beam-rocking illuminations.

For the past decade, revolutionary progress has been made in electron microscope instrumentation, in particular the innovative electron optics that corrects the spherical aberration ( $C_s$ ) of the objective lens<sup>3-5</sup>. At present both TEM and STEM routinely provide sub-ångström resolution<sup>25-27</sup>, and also significantly better sensitivity to detect the light atoms<sup>6-13</sup>.  $C_s$ -corrected TEM successfully identified local oxygen concentrations at individual atomic sites<sup>6</sup> and revealed detailed edge structure of graphene consisting of a carbon monolayer<sup>11</sup>. Remarkable observation comes from ADF STEM imaging of a monolayer boron nitride<sup>9</sup>, where individual boron and nitrogen as well as occasional carbon and oxygen impurity atoms are all simultaneously identified. Here, though, we should remember that the ADF contrast is based on scattering amplitude and known as atomic number  $Z$  contrast<sup>2</sup>, whose sensitivity depends on the scattering power of the relevant atoms. For detection of lighter atoms with extremely weak scattering, ABF phase-contrast imaging based on wave interference may be preferred, because it requires the object (atoms) only to alter the phase of a wave (weak-phase object<sup>21</sup>; WPO). In fact, significant sensitivity of ABF STEM was demonstrated by imaging oxygen<sup>7,8</sup> and nitrogen<sup>7</sup> atoms in crystalline solids, and further lithium atoms in a  $\text{LiV}_2\text{O}_4$  compound<sup>13</sup>. In the present work, using ABF STEM we demonstrate the first direct imaging of the lightest hydrogen atoms in a crystalline solid.

The optimum conditions of ABF STEM imaging can be derived on the basis of PCTF for the HCI TEM (refs 17,18). Again, reciprocity supports the equivalence between the techniques and practically holds within a weak-phase approximation (that is, specimen must be sufficiently thin to be treated as a WPO). Recently, characteristics of ABF imaging have been investigated on the basis of calculations of fast-electron propagations within the several compounds consisting of light atoms, and it is found that the light atoms can be visible over a wide range of specimen thickness even under strong dynamical diffraction conditions<sup>8</sup>. The present PCTF description aims to give more fundamental, straightforward insights into why ABF STEM is able to provide enhanced phase contrast in terms of the improved lens properties. Image formation of the phase contrast relies on a phase transfer of the scattered wave by the objective lens, which is described by the lens transfer function  $\exp(-i\chi(\mathbf{q}))$ , where  $\chi(\mathbf{q})$  is a wavefront aberration function of the scattering vector  $\mathbf{q}$ . PCTF is given as an imaginary part of the lens transfer function, and hence it results in  $\sin \chi(\mathbf{q})$  in the case of axial illumination. For off-axis HCI, the tilt-incident wave  $\mathbf{K}$  as well as the

<sup>1</sup>Department of Materials Science & Engineering, University of Tokyo, Tokyo 113-8656, Japan, <sup>2</sup>Electron Optics Division, JEOL Ltd., Tokyo 196-8558, Japan. \*e-mail: abe@material.t.u-tokyo.ac.jp.

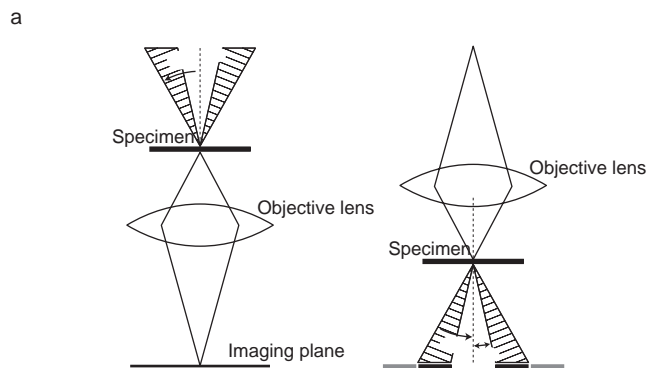


**Figure 1 | Schematic ray diagrams of HCl-TEM/ABF-STEM and PCTF of HCl.** **a**, HCl-TEM with the cone angle ranging from minimum  $\theta_c^{\min}$  to maximum  $\theta_c^{\max}$  is equivalent to ABF-STEM with the detector angle ranging from minimum  $\theta_d^{\min}$  to maximum  $\theta_d^{\max}$  ( $\theta_d^{\max}$  is set to a convergent semiangle  $\alpha$ ). **b**, HCl-PCTF calculated on the basis of equations (1) and (2), with  $\lambda = 2.5$  pm and  $C_5 = 1.5$  mm. Each of the dotted curves represents PCTF with the fixed  $\theta_c$  (equation (2)), and its corresponding first-cross point where the curve first becomes zero (second-cross means vice versa) is plotted for each, as shown at the upper right. Note that the first-cross points occur in the low-frequency region less than  $10 \text{ nm}^{-1}$  with  $\theta_c$  values larger than  $20 \text{ mrad}$ , around which the  $\theta_c^{\max}$  may well be optimized. The solid red curve shows the HCl-PCTF integrated over  $\theta_c^{\min} \sim \theta_c^{\max}$  (equation (1)). PCTF with axial illumination is shown by the solid blue curve, calculated with the representative aberration-corrected TEM parameters<sup>6</sup> ( $C_5 = -40 \mu\text{m}$ , defocus =  $9 \text{ nm}$ ,  $C_c = 1.4 \text{ mm}$ ), and the corresponding damping envelope<sup>30</sup> derived with the energy spread of the beam  $\Delta E = 0.3 \text{ eV}$  is shown by the dashed blue line. This PCTF is shown by inverted values for comparison with the present HCl-PCTF.

scattered wave  $\mathbf{k}$  is affected by the lens aberrations, and therefore the corresponding PCTF,  $L(\mathbf{q})$ , is written as<sup>17,19</sup>

$$L(\mathbf{q}) = \int_{\theta_c^{\min}}^{\theta_c^{\max}} \int_{\phi} \sin(\chi(\mathbf{k}) - \chi(\mathbf{K})) d\phi d\theta_c \quad (1)$$

where  $\phi$  represents an azimuth around the optical axis,  $\theta_c$  represents a cone angle ranging from  $\theta_c^{\max}$  to  $\theta_c^{\min}$  (Fig. 1a) and the scattering vector  $\mathbf{q}$  is defined as  $\mathbf{k} - \mathbf{K}$ . The third-order  $C_3$  becomes zero

after the aberration correction, and now the fifth-order spherical aberration  $C_5$  dominates the phase transfer of the lens. Therefore, with fixed  $\theta_c$ , PCTF is given as<sup>17,18</sup>

$$L(u, \theta_c) = \int \sin \frac{\pi}{3} C_5^5 \left\{ \left( \frac{u + \theta_c \cos \phi}{\lambda} \right)^2 + (\theta_c \sin \phi)^2 \right\}^6 - \theta_c^6 \} d\phi \quad (2)$$

where  $u$  represents the magnitude of  $\mathbf{q}$ , and  $\lambda$  is the wavelength of the accelerated electron. We have tuned the HCl conditions according to equations (1) and (2), and obtained the well-optimized PCTF with  $11 \text{ mrad} \leq \theta_c \leq 22 \text{ mrad}$ , as shown in Fig. 1b. Information transfer now remarkably extends up to  $22.5 \text{ nm}^{-1}$ , which is far beyond from that of the typical axial illumination ( $\sim 8 \text{ nm}^{-1}$ ) and corresponds to the real-space correlation length of  $44.4 \text{ pm}$ . It is noted that the entire shape of the HCl PCTF curve, like a gently sloped hill (Fig. 1b), may work effectively for increasing the visibility of the weak-scattering light atoms, given the condition that the phases of the wave are almost equivalently transferred over wide high-frequency ranges. This is similar to the previous description of the 'triangular shape'<sup>17</sup> of HCl PCTF, which was pointed out to suppress the possible artefacts and noise effectively.

Using the ABF condition with  $11 \text{ mrad} \leq \theta_d \leq 22 \text{ mrad}$  set up in accordance with the optimized HCl condition ( $11 \text{ mrad} \leq \theta_c \leq 22 \text{ mrad}$ ), we successfully imaged the hydrogen-atom columns in a crystalline compound. To provide a solid demonstration of hydrogen imaging, we chose the  $\text{YH}_2$  compound that is known as one of the most (thermodynamically) stable hydrides; see the van't Hoff plot for the hydride dissociation (Supplementary Fig. S1). In the plot, it is found that  $\text{YH}_2$  is the most stable among the several representative hydrides and never dissociates even under extremely low-pressure/high-temperature conditions (note that, within the microscope, the specimen is exposed to a very low pressure of the order of  $\sim 10^{-5} \text{ Pa}$ , which promotes hydrogen desorption for weakly bonded hydrides). In fact, it was indeed confirmed that the  $\text{YH}_2$  compound is remarkably stable even under the electron beam radiation with the present STEM conditions (probe diameter is approximately  $0.08 \text{ nm}$  with a current  $\sim 10 \text{ pA}$ ). No significant changes were observed in the image appearances, electron diffraction or electron energy loss spectroscopy, at least until a prolonged radiation of  $30 \text{ min}$  (Supplementary Figs S2 and S3). Details of the sample stability during the practical STEM beam radiations and the damage behaviours by the intense beam radiations were systematically investigated, including an estimation of critical electron doses to cause a structural damage/change; all of these results are described in Supplementary Information. On the basis of these careful evaluations of the  $\text{YH}_2$  robustness against the beam radiation, we concluded that knock-on damage events to eject hydrogen atoms hardly take place in the early period of the present STEM observation, during which the hydrogen atoms hence firmly stay in the compound.

The  $\text{YH}_2$  compound has a fluorite-type structure, for which the individual yttrium- and hydrogen-atom columns distinguishably appear along the  $[010]$  projection (Fig. 2a). Faint but distinct dark-dot contrast can be recognized at the hydrogen-atom column positions in the ABF image (Fig. 2b), the validity of which is well demonstrated by the averaged intensity profiles across the yttrium and hydrogen sites, as shown in Fig. 3a. We note that no significant intensity is observed at the relevant positions in the bright-field image (Fig. 2c) or the ADF image (Fig. 2d). It is therefore concluded that, only when the sufficiently extended PCTF is realized by HCl/ABF conditions, the hydrogen atoms can be successfully detected by phase-contrast imaging that reveals atoms as dark dots within a WPO approximation. According to the log-ratio method<sup>2b</sup> using electron energy loss spectroscopy, specimen thickness in the observed region (Fig. 2b) was estimated



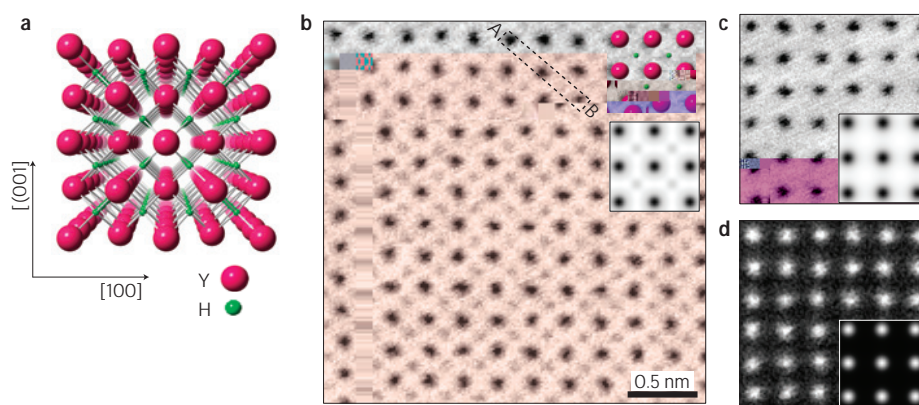


**Figure 2 | ABF, bright-field and ADF-STEM images of the crystalline compound  $\text{YH}_2$ .** **a**, Crystal structure of  $\text{YH}_2$  viewed from the [010] crystallographic direction. **b–d**, ABF (**b**), bright-field (**c**) and ADF (**d**) images obtained with the detector ranges ( $\theta_d^{\min} - \theta_d^{\max}$ ) 11–22 mrad, 0–22 mrad and 70–150 mrad, respectively. ABF (**b**) and ADF (**d**) images were simultaneously recorded with the detector configurations in Fig. 1a. Simulated images are inset in images **b–d**, and the  $\text{YH}_2$  unit-cell projection is overlaid in **b**.

to be approximately  $8 \pm 2$  nm, which is thin enough to apply a WPO approximation.

Image simulations based on the fast-Fourier-transform multislice algorithm<sup>29</sup> are carried out with the estimated thickness of 8 nm, reproducing fairly well all the observed features, ABF, bright-field and ADF STEM images, as inset in each of the images of Fig. 2b–d. It is also confirmed by the simulation of ABF imaging that no significant intensity occurs at the hydrogen sites when the hydrogen atoms are removed from the structure (that is, the hypothetical fluorite  $\text{YH}_2$  structure where all the hydrogen sites are vacant; see Supplementary Fig. S6). This strongly supports the validity that the observed intensity is indeed originated from the hydrogen atoms themselves, not by the imaging artefacts of phase contrast. A good match between the experiment and simulation is further confirmed by the corresponding intensity profiles shown in Fig. 3a, where the yttrium–hydrogen ABF-intensity profiles calculated with the relevant thicknesses ( $\sim 8$  nm) fit semiquantitatively with the experimental profile. We here note that, in the experimental ABF image, the intensity at the hydrogen sites was found to almost vanish in the thick region (estimated as about  $\sim 20$  nm) of the present cleavage wedge-shape specimen. This is confirmed by computing the thickness dependence of the ABF intensity (thickness map<sup>29</sup>) shown in Fig. 3b, in which the relative intensity between the yttrium and hydrogen alters with increasing thickness owing to dynamical diffraction effects. The hydrogen contrast becomes significantly weak around the thickness of 20 nm whose intensity profile is also shown in Fig. 3a, and with this condition the hydrogen intensity would be almost hidden in the background and hardly detected in the experiment. It is nevertheless noteworthy that both the yttrium and hydrogen sites never reveal contrast reversal (that is, the atom positions look like either dark or bright dots) but show simple intensity oscillations over a wide thickness range

(12 53 mrad) including outside the direct disc. These situations are in contrast with the present work, which further discusses why ABF-STEM works well for the detection of light elements in relation to the hollow-cone illumination TEM.

## Methods

We used an aberration-corrected STEM (JEM-ARM200F) operated at accelerating voltage 200 kV, equipped with a field-emission gun whose energy spread  $\Delta E$  is about 0.3 eV. The ABF STEM configuration in Fig. 1a was realized by masking the corresponding centre region of the bright-field detector. Parameter values during STEM observations were defocus  $\sim 0$  (nm),  $C_c \sim 0$  ( $\mu\text{m}$ ),  $C_c \sim 1.4$  mm and  $C_s \sim 1.5$  mm. These were used for the PCTF calculations and image computations. Specimens for STEM observation were prepared by crushing the bulk material and depositing it onto perforated amorphous carbon film supported on Cu grids. Thin areas for a WPO approximation are frequently realized around the edge of cleavage wedge-shape crystalline pieces, for which a surface amorphous layer and/or roughness that seriously affect the image contrast can be avoided owing to a cleavage process.

Received 18 October 2010; accepted 7 January 2011;  
published online 13 February 2011

## References

1. Crewe, A. V., Wall, J. & Langmore, J. Visibility of single atoms. *Science* **168**, 1338–1340 (1970).
2. Pennycook, S. J. & Boatner, L. A. Chemically sensitive structure-imaging with a scanning transmission electron microscope. *Nature* **336**, 565–567 (1988).
3. Haider, M. *et al.* Electron microscopy image enhanced. *Nature* **392**, 768–769 (1998).
4. Batson, P. E., Dellby, N. & Krivanek, O. L. Sub-ångström resolution using aberration corrected electron optics. *Nature* **418**, 617–620 (2002).
5. Sawada, H. *et al.* Correction of higher order geometrical aberration by triple 3-fold astigmatism field. *J. Electron Microsc.* **58**, 341–347 (2009).
6. Jia, C. L. & Urban, K. Atomic-resolution measurement of oxygen concentration in oxide materials. *Science* **303**, 2001–2004 (2004).
7. Okunishi, E. *et al.* Visualization of light elements at ultrahigh resolution by STEM annular bright field microscopy. *Microsc. Microanal.* **15**, 164–165 (2009).
8. Findlay, S. D. *et al.* Dynamics of annular bright field imaging in scanning transmission electron microscopy. *Ultramicroscopy* **110**, 903–923 (2010).
9. Krivanek, O. L. *et al.* Atom-by-atom structural and chemical analysis by annular dark-field electron microscopy. *Nature* **464**, 571–574 (2010).
10. Liu, Z. *et al.* Imaging the dynamic behaviour of individual retinal chromophores confined inside carbon nanotubes. *Nature Nanotech.* **2**, 422–425 (2007).
11. Girit, Ö. Ç. *et al.* Graphene at the edge: Stability and dynamics. *Science* **323**, 1705–1708 (2009).
12. Shao-Horn, Y., Croguennec, L., Delmas, C., Nelson, E. C. & O'Keefe, M. A. Atomic resolution of lithium ions in  $\text{LiCoO}_2$ . *Nature Mater.* **2**, 464–467 (2003).
13. Oshima, Y. *et al.* Direct imaging of lithium atoms in  $\text{LiV}_2\text{O}_4$  by spherical aberration-corrected electron microscopy. *J. Electron Microsc.* **59**, 457–461 (2010).
14. Meyer, J. C., Girit, C. O., Crommie, M. F. & Zettl, A. Imaging and dynamics of light atoms and molecules on graphene. *Nature* **454**, 319–322 (2008).

15. Mathews, W. W. The use of hollow-cone illumination for increasing image contrast in microscopy. *Trans. Am. Microsc. Soc.* **2**, 190–195 (1953).
16. Hanssen, K. J. & Trepte, L. Die Kontrastübertragung im elektronemikroskop bei partiell kohärenterbeleuchtung (in German). *Optik* **33**, 166–181 (1971).
17. Rose, H. Nonstandard imaging methods in electron microscopy. *Ultramicroscopy* **2**, 251–267 (1977).
18. Dinges, C., Kohl, H. & Rose, H. High-resolution imaging of crystalline objects by hollow-cone illumination. *Ultramicroscopy* **55**, 91–100 (1994).
19. Rose, H. Phase-contrast in scanning transmission electron microscopy. *Optik* **39**, 416–436 (1974).
20. Cowley, J. M., Hansen, M. S. & Wang, S.-Y. Imaging modes with an annular detector in STEM. *Ultramicroscopy* **58**, 18–24 (1995).
21. Cowley, J. M. Image contrast in a transmission scanning electron microscope. *Appl. Phys. Lett.* **15**, 58–59 (1969).
22. Scherzer, O. The theoretical resolution limit of the electron microscope. *J. Appl. Phys.* **20**, 20–29 (1949).
23. Komoda, T. Electron microscopic observation of crystal lattices on the level with atomic dimension. *Jpn. J. Appl. Phys.* **5**, 603–607 (1966).
24. Kunath, W., Zemlin, F. & Weiss, K. Apodization in phase-contrast electron microscopy realized with hollow-cone illumination. *Ultramicroscopy* **16**, 123–138 (1985).
25. O'Keefe, M. A. *et al.* Sub-ångström high-resolution transmission electron microscopy at 300 keV. *Ultramicroscopy* **89**, 215–241 (2001).
26. Nellist, P. D. *et al.* Direct sub-ångström imaging of a crystal lattice. *Science* **305**, 1741 (2004).
27. Sawada, H. *et al.* STEM imaging of 47 pm-separated atomic columns by a spherical aberration-corrected electron microscope with a 300-kV cold field emission gun. *J. Electron Microsc.* **58**, 357–361 (2009).
28. Egerton, R. F. *Electron Energy-Loss Spectroscopy in the Electron Microscope* 2nd edn (Plenum, 1996).
29. Ishizuka, K. A practical approach for STEM image simulation based on the FFT multislice method. *Ultramicroscopy* **90**, 71–83 (2002).
30. Kabius, B. *et al.* First application of Cc-corrected imaging for high-resolution and energy-filtered TEM. *J. Electron Microsc.* **58**, 147–155 (2009).
31. Findlay, S. *et al.* Direct imaging of hydrogen within a crystalline environment. *Appl. Phys. Express* **3**, 116603 (2010).

## Acknowledgements

R.I. was supported as a Japan Society for the Promotion of Science research fellow. E.A. acknowledges support from a Grant-in-Aid for Scientific Research on Priority Areas 'Atomic scale modification' from the Ministry of Education, Culture, Sports, Science and Technology of Japan.

## Author contributions

E.A. initiated and designed the research, interpreted the data and wrote the paper. R.I. designed the experiments, analysed the data and carried out computer simulations. E.O., R.I. and E.A. carried out electron microscope experiments. H.S., Y.K. and F.H. contributed to interpretations of ABF imaging.

## Additional information

The authors declare no competing financial interests. Supplementary information accompanies this paper on [www.nature.com/naturematerials](http://www.nature.com/naturematerials). Reprints and permissions information is available online at <http://npg.nature.com/reprintsandpermissions>. Correspondence and requests for materials should be addressed to E.A.